

The Effect of the Approach to Gas Disk Gravitational Instability on the Rapid Formation of Gas Giant Planets

Alan P. Boss

*Department of Terrestrial Magnetism, Carnegie Institution for Science, 5241 Broad Branch
Road, NW, Washington, DC 20015-1305*

aboss@carnegiescience.edu

ABSTRACT

Observational evidence suggests that gas disk instability may be responsible for the formation of at least some gas giant exoplanets, particularly massive or distant gas giants. With regard to close-in gas giants, Boss (2017) used the β cooling approximation to calculate hydrodynamical models of inner gas disk instability, finding that provided disks with low values of the initial minimum Toomre stability parameter (i.e., $Q_i < 2$ inside 20 au) form, fragmentation into self-gravitating clumps could occur even for β as high as 100 (i.e., extremely slow cooling). Those results implied that the evolution of disks toward low Q_i must be taken into account. This paper presents such models: initial disk masses of $0.091 M_\odot$ extending from 4 to 20 au around a $1 M_\odot$ protostar, with a range (1 to 100) of β cooling parameters, the same as in Boss (2017), but with all the disks starting with $Q_i = 2.7$, i.e., gravitationally stable, and allowed to cool from their initial outer disk temperature of 180 K to as low as 40 K. All the disks eventually fragment into at least one dense clump. The clumps were again replaced by virtual protoplanets (VPs) and the masses and orbits of the resulting ensemble of VPs compare favorably with those of Boss (2017), supporting the claim that disk instability can form gas giants rapidly inside 20 au, provided that sufficiently massive protoplanetary disks exist.

Subject headings: accretion, accretion disks – hydrodynamics – instabilities – planets and satellites: formation – protoplanetary disks

1. Introduction

The spectacular success of the *Kepler* Mission (Borucki et al. 2010, 2011a,b) has revealed that super-Earth exoplanets are commonplace and apparently considerably more abundant

than gas giants, at least for short period orbits. While core accretion appears to be the dominant formation mechanism for the exoplanets discovered to date, there is observational evidence suggesting that disk instability may also play a role, at least for the formation of massive or distant gas giants. As a result, hybrid exoplanet population synthesis models (e.g., Boss 1998; Nayakshin 2010), combining both core accretion (e.g., Mizuno 1980; Pollack et al. 1996) and disk instability (e.g., Cameron 1978; Boss 1997), may be needed to explain the plethora of exoplanetary system discoveries. Boss (2017) summarized the observations supporting such a role for disk instability in gas giant planet formation, including protoplanetary disk masses, temperatures, and lifetime estimates, as well as the demographics of mature exoplanets and evidence for large protoplanets embedded in protoplanetary disks.

Further observational evidence in support of disk instability has continued to accumulate since Boss (2017), from both exoplanet demographics and protoplanetary disk studies. Host stars with high metallicities presumably are accompanied by metal-rich protoplanetary disks, and hence are believed to favor the core accretion mechanism. Stellar metallicities have often been touted as the definitive test of giant planet formation mechanisms (e.g., Fischer & Valenti 2005). However, recently analyses of stellar metallicities point to the need for a hybrid formation theory (e.g., Santos et al. 2017). Schlaufman (2018) showed that for solar-type stars, the distribution of transiting exoplanet masses as a function of stellar metallicity breaks up into two groups, with a break between about $4 M_{Jup}$ and $10 M_{Jup}$: exoplanets with masses below about $4 M_{Jup}$ preferentially orbit metal-rich stars, while those with masses above $10 M_{Jup}$ do not, implying a role for disk instability in forming the latter population. Narang et al. (2018) similarly found a break at $4 M_{Jup}$, with host star metallicity dropping as the transiting exoplanet mass increases above this value. Goda & Matsuo (2019) found that early-type stars can have massive exoplanets even for low metallicities. Maldonado et al. (2019) confirmed that host star metallicities drop as exoplanet masses increase, implying a role for disk instability for the more massive exoplanets.

Many examples of protoplanetary disks with rings, or even grand spiral arms, have been imaged by the ALMA DSHARP survey (e.g., Huang et al. 2018), indicative of marginally gravitationally unstable disks, the rapid formation of massive planets that created and shaped the rings, or both processes. The Elias 2-24 disk appears to host several gas giant planets (Cieza et al. 2017) at distances of 20, 52, and 87 au. The Elias 2-27 disk seems to contain a massive gas giant planet formed by disk instability (Meru et al. 2017), though controversy continues over the source of the spiral arms (e.g., Forgan et al. 2018; Dong et al. 2018). The ongoing Subaru SEEDS survey has found nine distant companion candidates to date out of 68 young stellar objects studied (Uyama et al. 2017). Clarke et al. (2018) presented ALMA images arguing for the presence of four gas giant planets in the CI Tau disk, at an age of only 2 Myr, at orbital distances including $\sim 13, 39,$ and 100 au. The Herbig

A5 star MWC 758 appears to be orbited by a dust transition disk shepherded by an inner (35 au) $1.5-M_{Jup}$ planet and by an outer (140 au) $5-M_{Jup}$ planet (Baruteau et al. 2019). Two accreting protoplanets have been imaged around the young star PDS 70 (Haffert et al. 2019), with masses in the range of 4 to 17 M_{Jup} and 4 to 12 M_{Jup} , and orbital distances of ~ 21 au and ~ 35 au, respectively. Core accretion has difficulties explaining the rapid formation of gas giant planets at such distances, compared to disk instability (e.g., Chambers 2006, 2016; Coleman & Nelson 2016; cf. Boss 2011). Indeed, forming distant gas giants by disk instability has become conventional wisdom (e.g., Boley 2009; Nero & Bjorkman 2009; Meru & Bate 2010; Kratter & Murray-Clay 2011; Rogers & Wadsley 2012; Vorobyov 2013; Madhusudhan et al. 2014; Rice et al. 2015; Young & Clarke 2016; Muller et al. 2018).

This paper extends upon the work by Boss (2017), who used the β cooling approximation for disk thermodynamics to study the fragmentation process in disks with a wide range of β values (1 to 100), starting either close to gravitational instability (Toomre $Q_{min} = 1.3$) or gravitationally stable ($Q_{min} = 2.7$). Boss (2017) found that fragmentation could occur even for high $\beta = 100$, provided that the disk had a low initial value of $Q_{min} < 2$. The question of disk fragmentation then becomes one of whether protoplanetary disks can evolve into low Q , unstable configurations, or whether the spiral arms that inevitably form first would transfer mass and angular momentum fast enough to prevent fragmentation and dense clump formation, as is commonly believed to be the case (e.g., Nixon et al. 2018).

The purpose of the present paper is thus to examine the basic question of the approach to gas disk gravitational instability in disks which are cooling from an initially gravitationally stable configuration. The models start from the $Q_{min} = 2.7$ model of Boss (2017), with the same range of β values, but with the minimum disk temperature constraints relaxed to 40 K (i.e., relaxed to that of the outer disk minimum temperature for the unstable models with initial $Q_{min} = 1.3$). These models thus study the effect of varied cooling rates on the approach to a gravitationally unstable phase of disk evolution.

2. Radiative Transfer and Beta Cooling Models

The inner regions of protoplanetary gas disks massive enough to become gravitationally unstable are optically thick, requiring radiative transfer to model the energy lost by disk radiation to the infalling protostellar envelope. Boss (2001) calculated the first disk instability models including radiation transfer in the diffusion approximation, finding that fragmentation into dense clumps could occur in low Q_{min} disks. Reviews by Durisen et al. (2007) and Helled et al. (2014) summarized the work on two- and three-dimensional hydrodynamical models of disk instability, illustrating a variety of reasons for different results regarding

fragmentation, ranging from the numerical grid resolutions of finite difference codes and the smoothing lengths for smoothed-particle hydrodynamics (SPH) codes, to the accuracies of their gravitational potential solvers. The reviews concluded in part that the radiative transfer solver appeared to be critical to disk fragmentation, which requires the disk to remain sufficiently cold for spiral arms to form self-gravitating, contracting, dense clumps. Testing the radiative transfer codes against analytical solutions has not resolved all the issues, e.g., Boley & Durisen (2006) showed agreement of their cylindrical coordinate code with an analytical solution, while Boss (2009) found agreement with his spherical coordinate code with two other analytical radiative transfer solutions.

As a result of this impasse, and considering the heavy computational overhead of three-dimensional radiative transfer, even in the diffusion approximation, attention has turned to more simplified methods for representing disk cooling processes. Gammie (2001) was the first to propose that the outcome of gas disk gravitational instability depended primarily on the beta parameter $\beta = t_{cool}\Omega$, where t_{cool} is the disk cooling time and Ω is the disk local angular velocity. When $\beta < 3$, Gammie (2001) suggested that the disk would fragment. As a result, a critical value of $\beta_{cr} = 3$ has become a standard for predicting the outcome of the fragmentation process in protoplanetary disks. However, subsequent work by many groups (as summarized in Boss 2017) has questioned whether or not the value of $\beta_{cr} = 3$ is a correct indicator for disk fragmentation, with other estimates of the true value ranging from $\beta_{cr} \sim 10$ to $\beta_{cr} \sim 30$, depending on the details of the numerical code used, such as numerical resolution and the artificial viscosity for SPH codes. More recently, Deng et al. (2017) found evidence for $\beta_{cr} = 3$ for a novel meshless finite mass (MFM) code, but not for a SPH code, the latter apparently a result of artificial viscosity. Baehr et al. (2017) used local three-dimensional disk simulations to find $\beta_{cr} \sim 3$. Mercer et al. (2018) showed which of two approximate radiative transfer procedures is more accurate for protostellar disks, and demonstrated that the effective value of β in such disks could vary from ~ 0.1 to ~ 200 , i.e., a single, constant value of β may not be capable of representing the full range of physical conditions in gravitationally unstable disks.

3. Numerical Methods and Initial Conditions

The numerical code is the same as that used by Boss (2017), which can be consulted for relevant details. The EDTONS code solves the three-dimensional equations of hydrodynamics and the Poisson equation for the gravitational potential, with second-order-accuracy in both space and time, on a spherical coordinate grid (see Boss & Myhill 1992). Note that an explicit artificial viscosity is not used in the models. Boss (2017) described how the

β cooling approximation was incorporated into the solution of the specific internal energy equation (Boss & Myhill 1992), where the time rate of change of energy per unit volume, which is normally taken to be that due to the transfer of energy by radiation in the diffusion approximation, is defined in such a way that only cooling is permitted.

In the Boss (2017) models, the disk temperatures at given radial distances from the central protostar were not allowed to fall below their initial values, which meant that initially warm and hot disks could not become any cooler than in their initial state, independent of the value of β . Those disks could only approach gravitational instability by transporting disk mass inward so that the local gas disk surface density increased. This same minimum temperature constraint was imposed in all of the previous disk instability models in this series (see Boss 2017), and so was retained to allow comparisons with the earlier work. Here, though, we modify this constraint to allow disks to cool down to 40 K, regardless of the initial radial temperature profile, which has a minimum of 180 K. Figure 1 shows the initial temperature profile and minimum temperature constraint for all the models. The profile decreases monotonically with radial distance from the initial maximum of 600 K at 4 au.

As in Boss (2017), the equations are solved on a grid with $N_r = 100$ or 200 uniformly spaced radial grid points, $N_\theta = 23$ theta grid points, distributed from $\pi/2 \geq \theta \geq 0$, but compressed toward the disk midplane, and $N_\phi = 512$ or 1024 uniformly spaced azimuthal grid points. The radial grid extends from 4 to 20 au, with disk gas flowing inside 4 au being added to the central protostar. The gravitational potential is obtained through a spherical harmonic expansion, including terms up to $N_{Ylm} = 48$. The r and ϕ numerical resolutions are doubled when needed to avoid violating the Jeans length (e.g., Boss et al. 2000) and Toomre length criteria (Nelson 2006). If either of these two criteria is violated, the calculation stops, and the spatial resolution is doubled in the relevant direction by dividing each cell into half while conserving mass and momentum. When dense clumps form, eventually the Jeans and Toomre length criteria will be violated at their density maxima, even with $N_r = 200$ and $N_\phi = 1024$. The cell with the maximum density is then drained of 90% of its mass and momentum, which is then inserted into a virtual protoplanet (VP, Boss 2005). These VPs orbit in the disk midplane, subject to the gravitational forces of the disk gas, the central protostar, and any other VPs, while the disk gas is subject to the gravity of the VPs. Those VPs that reach the the inner or outer boundaries are removed from the calculation. The VPs gain mass at the rate (Boss 2005, 2013) given by the Bondi-Hoyle-Lyttleton (BHL) formula (e.g., Ruffert & Arnett 1994), as well as the angular momentum of any accreted disk gas. The VPs are thus handled identically to their treatment in Boss (2017).

As in Boss (2017), the initial gas disk density distribution is that of an adiabatic, self-gravitating, thick disk in near-Keplerian rotation about a stellar mass M_s (Boss 1993), with

an initial midplane density chosen to enforce near-Keplerian rotation. The inner disk radius is 4 au, and the outer disk radius is 20 au. The initial disk mass M_d is then $0.091 M_\odot$, and the initial protostellar mass is $M_s = 1.0 M_\odot$. The initial outer disk temperature is set to 180 K for all models, so that all begin from a gravitationally stable configuration with an initial minimum value of the Toomre (1964) Q gravitational stability parameter of 2.7. Only the value of β was varied in the models (Table 1), with the same eight values used as in Boss (2017): 1, 3, 10, 20, 30, 40, 50, and 100.

Cieza et al. (2018) used ALMA to show that FU Orionis disks have radii less than 20 to 40 au and masses of 0.08 to $0.6 M_\odot$. Such disks are the observational analogs of the marginally gravitationally unstable disks to be studied here.

4. Results

Table 1 lists the basic results for all of the models: the final times reached, the final and maximum number of virtual planets (N_{VP}) that formed, and the amount of disk mass lost by accretion onto either the VPs or the central protostar, in Jupiter mass units. The final times reached ranged from 288 yrs to 462 yrs, similar to the results of Boss (2017). The initial orbital period of the disk at the inner edge is 8.0 yr and 91 yrs at the outer edge, so clearly the models spanned a time period long enough for many revolutions in the inner disk, and multiple revolutions in the outer disk. Each model required over one year of time to compute, each running on a separate, single core of the Carnegie memex cluster at Stanford University.

4.1. Model be5

Figures 2 and 3 present the results for model be5, which is typical of the results for all of the models here. Figure 2 shows that the initially nearly axisymmetric gas disk begins to form strong spiral arms just outside the hot inner disk, and these arms continue to grow and extend to the outer disk. By the end of the evolution, the arms are dominated by $m = 1$ one-armed spirals, with maximum amplitude $a_{max} \approx 1.4$, along with $m = 2$ two-armed spirals with $a_{max} \approx 0.5$ and $m = 3$ three-armed spirals with $a_{max} \approx 0.3$. The caption for Figure 2 lists the maximum midplane densities reached, which started at $1.0 \times 10^{-10} \text{ g cm}^{-3}$, and rose as high as $2.6 \times 10^{-9} \text{ g cm}^{-3}$ after 162 yrs for the densest clump seen in Figure 2b. These clump densities should be compared to the relevant free fall times when considering whether the clumps might contract to even higher densities and survive as VPs. The free fall

time (t_{ff}) for a pressure-less, uniform density (ρ) gas sphere is $t_{ff} = (3\pi/32G\rho)^{1/2}$, where G is the gravitational constant. For $\rho = 10^{-10}$ g cm $^{-3}$, $t_{ff} = 6.7$ yrs, while for $\rho = 10^{-9}$ g cm $^{-3}$, $t_{ff} = 2.1$ yrs. Clearly the clumps formed in model be5 reach maximum densities high enough to plausibly contract to higher densities on time scales considerably less than a single orbital period at their orbital distances, which are about 12 au for Figure 2b, where the orbital period is ~ 40 yrs.

Figure 3 shows the midplane temperature evolution, starting from 180 K outside the hot inner disk, and cooling down to as low as 40 K in the outer disk after ~ 162 yrs. For model be5, with $\beta = 30$, $t_{cool} = \beta/\Omega = \beta P/(2\pi) \approx 4.8P$, where P is the local disk rotation period. Given the initial disk rotation periods of 8.0 yrs at the inner edge and 91 yrs at the outer edge, the nominal cooling times for model be5 are then about 38 yrs at the inner edge and 436 yrs at the outer edge. The cooling time is coded (Boss 2017) as being the ratio of the specific internal energy to the time rate of change of the specific internal energy. With that definition, and in the absence of compressional or other heating terms, the specific internal energy could formally drop to zero in one cooling time. Hence the rate of inner and outer disk cooling seen in the models can be understood in the manner that β cooling was defined in both the present and 2017 models. Note that the innermost disk forms high temperature spiral features on top of the hot inner disk minimum temperature constraint, though the inner gas disk remains relatively featureless in Figure 2, compared to the outer disk.

4.2. VPs Formation and Evolution

The maximum midplane density in model be5 in Figure 2b occurs in the clump located close to 12 noon at an orbital radius of ~ 10 au. The disk gas has a maximum temperature of ≈ 100 K at the maximum density of 2.6×10^{-9} g cm $^{-3}$ at 162 yrs, yielding a Jeans mass of $\approx 1.2 \times 10^{30}$ g, or about $0.6 M_{Jup}$. The mass of this densest clump is $\approx 1.3 \times 10^{30}$ g, or about $0.65 M_{Jup}$, making the clump marginally gravitationally bound. Shortly after 162 yrs, the clump maximum density exceeds the Toomre criterion, and as the model had already been refined to the highest spatial resolution, a VP was inserted in the center of the clump with an initial mass of $\sim 0.001M_{Jup}$, 90% of the mass within the cell with the maximum midplane density. The VP thereafter orbits the central protostar and rapidly accretes disk gas and orbital angular momentum, as shown in Figure 4, at the Bondi-Hoyle-Littleton rate (Ruffert & Arnett 1994). Figure 4 displays the masses of all the VPs formed during the evolution of model be5, which at one time (Table 1) had as many as five VPs in orbit, though only a single VP was still active at the end of the evolution at 422 yrs. The others hit either the inner (4 au) or outer (20 au) grid boundary, and were thereafter dropped from consideration.

Note that in a more realistic disk model, VPs that encounter these artificial orbital limits need not be lost altogether, as they may very well orbit for significant periods without being accreted by the central protostar, or ejected from the system by mutual close encounters.

Figure 4 shows that some of the VPs in model be5 gained mass at the rate of about $1 M_{Jup}$ per 100 yrs, or $\sim 1 \times 10^{-2} M_{Jup} \text{ yr}^{-1}$. This rate is considerably higher than estimated mass accretion rates for observed accreting young companions embedded in circumstellar disks, where objects with masses of $\sim 10 M_{Jup}$ accrete no faster than $\sim 1 \times 10^{-6} M_{Jup} \text{ yr}^{-1}$ (e.g., Cugno et al. 2019). However, the very fact that these observational estimates were based on direct imaging of young companions implies that these circumstellar disks are not as optically thick, and hence not as massive, as the protoplanetary disks modeled here, as well as being objects at much later phases of evolution than the newly-formed VPs studied here. Model be5 formed VPs with a total mass of $\sim 4 M_{Jup}$ by the end of the calculation. Table 1 shows that the model be5 disk lost $4.5 M_{Jup}$ during the evolution, so most of this mass loss went to VP formation, and only $\sim 0.5 M_{Jup}$ was accreted by the central protostar. The central protostar mass accretion rate was thus $\sim 10^{-6} M_{\odot} \text{ yr}^{-1}$, a typical rate for a marginally gravitationally unstable disk. In comparison, T Tauri stars and FU Orionis outburst stars have mass accretion rates of $\sim 10^{-7} M_{\odot} \text{ yr}^{-1}$ and $\sim 10^{-4} M_{\odot} \text{ yr}^{-1}$, respectively (e.g., Hartmann & Kenyon 1996).

Figure 5 presents the results for the VPs formed in all eight models listed in Table 1, showing similar behavior as in model be5: many VPs form, but only a fraction survive long enough to accrete sufficient gas to reach gas giant planet masses. Figure 5 is quite similar to the corresponding Figure 8a in Boss (2017), showing the results for the varied β cooling models where the midplane temperatures were not allowed to drop below the initial values, for the model with the lowest outer disk initial temperature (40 K, compared to 180 K here). The results suggest that disk instability can form dense clumps in either case: starting with a relatively cold disk with a range of β values (Boss 2017), or starting with a relatively warm disk and waiting for β cooling to increase the degree of gravitational instability of the disks.

Figure 6 shows the results for all eight models in terms of the evolution of the orbital radii of the VPs that form. Formation occurs in the disk sweet spot between about 6 au and 10 au, where the midplane temperatures are not as high as in the inner disk (e.g., Figure 3), the midplane densities are high, and the orbital period (~ 20 yr) is shorter than in the outer disk (~ 90 yr). While a significant fraction manage to continue to orbit in the sweet spot, 73 VPs reach the inner boundary at 4 au, while another 27 strike the outer boundary, as noted in Table 1. The VPs migrate as a result of the gravitational torques they receive from the evolving disk spiral arms (e.g., Figure 2), as well as from close encounters with each other. Again, this behavior is quite similar to that of the corresponding models in Boss

(2017, Figure 8b). The circled points in Figure 6 show the final locations of the VPs, which are distributed more or less uniformly throughout the disk.

Figure 7 shows the masses and orbital radii of all of the VPs from the present set of models, sampled periodically throughout the evolutions, and plotted as in Figure 9 of Boss (2017). For comparison, Figure 8 shows the known exoplanets as of July 10, 2019, from the Extrasolar Planets Encyclopedia (exoplanets.eu). Table 2 shows the percentage of the total number of exoplanets in Figures 7 and 8 with masses above $\approx 0.1M_{Jup}$ broken up into separation bins of 2 au. It will be seen that the two distributions look reasonably similar for semi-major axes less than about 8 au, as was the case for the Boss (2017) models. Note also that the present models sample only the effects of varying the disk cooling rate, just one parameter out of the many that may need to be varied to reproduce exoplanet demographics (e.g., disk and stellar masses). The results shown in Figure 7 are also broadly consistent with the results of the disk instability models by Forgan et al. (2015), though a direct comparison is not appropriate, as they considered disks with radii of 100 au, five times larger than the present models.

Finally, Table 1 demonstrates that though all the models started with identical initial conditions, the models with the lower β values fragmented into considerably larger numbers of VPs than the higher β models, as expected. They also lost considerably more VPs to migrations into the grid boundaries, consistent with their greater numbers formed and more vigorous spiral arms, which are the principal agent of VP orbital migration, as the mass in any individual spiral arm is typically greater than that of the most massive VPs that form. Nevertheless, it is remarkable that even the models with the highest values of β still fragmented into at least one dense clump that required the formation of a VP, and that in each model, at least one VP remained active at the end of the calculations. Allowing the disks to slowly cool down to 40 K was critical for obtaining spiral arm formation and eventual dense clump formation to occur in the models with large values of β ; the Boss (2017) models with large β values did not fragment when the disk was prevented from cooling to such a low temperature. Midplane temperatures of 40 K at 10 au are consistent with spectral energy distributions for T-Tauri-star disks (Lachaume et al. 2003; DAlessio et al. 2006).

The results imply that the choice of the value of β for disk fragmentation may not be as critical as has been generally assumed or found to be the case. As noted in the Introduction and summarized in Boss (2017), many papers have questioned whether the Gammie (2001) value of $\beta_{cr} = 3$ is a universal criterion, given that other estimates range from ~ 10 to ~ 30 and depend on the details of the numerical code used. E.g., Gammie (2001) used a razor-thin (2D) numerical model in the shearing-sheet approximation, which can only represent a small region of a large-scale disk. Considering that the clumps formed in the present

models result from the interactions of large-scale spiral arms (Figure 2), it is hard to see how a local analysis could be relevant for such large-scale fragmentation. While Rice et al. (2003) used 3D SPH disk models to confirm Gammie’s basic claim with a higher value of $\beta_{cr} \sim 6$, their models were limited to a rather low resolution of 250,000 ($\sim 64^3$) particles, limiting the code’s ability to achieve convergence. In contrast, the present models employ $N_\phi = 512$ and 1024 in the coordinate critical for the growth of non-axisymmetric structures. Meru & Bate (2011b) found that convergence was not achieved for SPH models with as many as 16,000,000 particles, finding that fragmentation occurred for larger β values as the resolution was increased, leading them to doubt whether a critical value of β exists. Meru & Bate (2011a) found that estimates of β_{cr} also depend on the assumed underlying disk density profile, again arguing against the generality of a specific value for β_{cr} . Further comments about previous β -cooling models may be found in Boss (2017).

Boss (2017) summarized the state of radiative transfer models of disk instability, which should yield a more correct handling of disk thermodynamics than simple β cooling models. As noted in the reviews by Durisen et al. (2007) and Helled et al. (2014), the outcome of radiation hydrodynamics (RHD) disk instability models appears to be dependent on a range of numerical factors. Even when RHD codes are tested against analytical solutions, a clear decision need not result (e.g., cf. Boley & Durisen 2006, Boss 2009). Boley (2009) demonstrated that large-scale fragmentation is possible with his RHD code, using an azimuthal resolution of $N_\phi = 512$, when initially isothermal disks with radii of ~ 300 au are formed from gas infalling beyond 60 au from the central protostar. No fragmentation inside ~ 20 au was observed, as there was negligible disk mass in the inner regions, by design of the numerical experiment. Stamatellos & Whitworth (2008) presented two SPH RHD models of disks with radii of 40 au that did not undergo fragmentation. However, their two models were limited to 200,000 particles representing the gas disk, which appears to be insufficient for achieving convergence. Finally, Mercer et al. (2018) found that their RHD results implied that the effective value of β varied throughout the disk, from ~ 0.1 to ~ 200 , an even wider range than studied in the present set of models.

5. Conclusions

These models are intended to be first steps toward creating a hybrid model for exoplanet population synthesis, where a combination of core accretion and disk instability works in tandem to try to reproduce the exoplanet demographics emerging from numerous large surveys using ground-based Doppler spectroscopy and gravitational microlensing or space-based transit photometry (e.g., *Kepler*, TESS).

The Boss (2017) models showed that the outcome of a phase of disk gravitational instability depends more strongly on the initial conditions adopted for the models than on the assumed disk cooling rate β . The present models have studied the evolution of protoplanetary disks into gravitationally unstable configurations, which is evidently just as important a factor as the disk cooling process. Remarkably, the models have shown that starting from a gravitationally stable, high Toomre Q disk, disks with a large range of cooling rates, from $\beta = 1$ to 100 (Table 1), eventually become gravitationally unstable, form numerous spiral arms, and then dense clumps requiring the insertion of VPs representing newly formed gas giant protoplanets. In combination with the results of Boss (2017), the models imply that protoplanetary disks with masses of $\sim 0.1M_{\odot}$ (e.g., FU Orionis star disks) should be able to form gas giants in the region from ~ 4 au to ~ 20 au. This implies the existence of a largely unseen population of gas giants orbiting solar-type stars, which could be detected by the gravitational microlensing survey and coronagraphic direct imaging technology efforts of the NASA WFIRST space mission, slated for launch around 2025.

In order to continue to study the viability of the disk instability mechanism for giant planet formation, the author is currently computing several other suites of protoplanetary disk models. One set is a continuation of the β cooling models presented here, but with a significant further enhancement of the highest spatial resolution permitted before the VP artifice is employed. While the present models were restricted to a maximum of 200 radial and 1024 azimuthal grid points before VP insertion, the suite currently running doubles both of these maxima, to 400 in radius and 2048 in azimuth. These are the highest spatial resolution grid models run to date with the EDTONS code, but at a penalty of running about eight times slower than the highest resolution models presented in this paper (time step halved for four times as many grid points). The second set was noted previously by Boss (2017), and these are flux-limited diffusion approximation (FLDA) models, starting with the same initial conditions as the present suite of models. The FLDA models run considerably slower than β cooling models for the same grid resolution, and hence the FLDA models are still in progress. The goal of this second suite is to compare the FLDA results with those of the β cooling models, at the same spatial resolution and same initial conditions, to attempt to determine if there is an optimal value of β that could be used in future disk instability models, thereby avoiding the computational burden associated with the FLDA approach.

The referee provided a number of helpful suggestions for improving the manuscript. The calculations were performed on the Carnegie memex cluster at Stanford University. I thank Michael Acierno and Floyd Fayton for their able assistance with the use of memex.

REFERENCES

- Baehr, H., Klahr, H., & Kratter, K. M. 2017, *ApJ*, 848, 40
- Baroteau, C., Barraza, M., Perez, S., et al. 2019, *MNRAS*, 486, 304
- Boley, A. C. 2009, *ApJ*, 695, L53
- Boley, A. C., & Durisen, R. H. 2006, *ApJ*, 641, 534
- Borucki, W., et al. 2010, *Science*, 327, 977
- Borucki, W., et al. 2011a, *ApJ*, 728, 117
- Borucki, W., et al. 2011b, *ApJ*, 736, 19
- Boss, A. P. 1993, *ApJ*, 417, 351
- Boss, A. P. 1997, *Science*, 276, 1836
- Boss, A. P. 1998, *ApJ*, 503, 923
- Boss, A. P. 2005, *ApJ*, 629, 535
- Boss, A. P. 2009, *ApJ*, 694, 107
- Boss, A. P. 2011 *ApJ*, 731, 74
- Boss, A. P. 2013, *ApJ*, 764, 194
- Boss, A. P. 2017, *ApJ*, 836, 53
- Boss, A. P., & Myhill, E. A. 1992, *ApJS*, 83, 311
- Boss, A. P., Fisher, R. T., Klein, R. I., & McKee, C. F. 2000, *ApJ*, 528, 325
- Cameron, A. G. W. 1978, *Moon Planets*, 18, 5
- Chambers, J. E. 2006, *ApJL*, 652, L133
- Chambers, J. E. 2016, *ApJ*, 825, 63
- Cieza, L. A., Cassassus, S., Perez, S., et al. 2017, *ApJL*, 851, L23
- Cieza, L. A., Ruiz-Rodriguez, D., Perez, S., et al. 2018, *MNRAS*, 474, 4347
- Clarke, C. J., Tazzari, M., Juhasz, A., et al. 2018, *ApJL*, 866, L7
- Coleman, G. A. L., & Nelson, R. P. 2016, *MNRAS*, 460, 2779
- Cugno, G., Quanz, S. P., Hunziker, S., et al. 2019, *A&A*, 622, A156
- DAlessio, P., Calvet, N., Hartmann, L., Franco-Hernandez, R., & Servin, H. 2006, *ApJ*, 638, 314
- Deng, H., Mayer, L., & Meru, F. 2017, *ApJ*, 847, 43

- Dong, R., Najita, J. R., & Brittain, S. 2018, *ApJ*, 862, 103
- Durisen, R. H., Boss, A. P., Mayer, L., et al. 2007, in *Protostars and Planets V*, ed. B. Reipurth, D. Jewitt, & K. Keil (Tucson, AZ: Univ. Arizona Press), 607
- Fischer, D. A., & Valenti, J. 2005, *ApJ*, 622, 1102
- Forgan, D. H., Hall, C., Meru, F., & Rice, W. K. M. 2018, *MNRAS*, 474, 5036
- Forgan, D., Parker, R. J., & Rice, K. 2015, *MNRAS*, 447, 836
- Gammie, C. F. 2001, *ApJ*, 553, 174
- Goda, S., & Matsuo, T. 2019, *ApJ*, 876, 23
- Haffert, S. Y., Bohn, A. J., de Boer, J., et al. 2019, *Nature Astronomy*, 10.1038/s41550-019-0780-5
- Hartmann, L., & Kenyon, S. J. 1996, *ARAA*, 34, 207
- Helled, R., Bodenheimer, P., Podolak, M., et al. 2014, in *Protostars and Planets VI*, ed. H. Beuther et al. (Tucson, AZ: Univ. Arizona Press), 643
- Huang, J., Andrews, S. M., Perez, L. M., et al. 2018, *ApJL*, 869, L43
- Kratter, K. M., & Murray-Clay, R. A. 2011, *ApJ*, 740, 1
- Lachaume, R., Malbet, F., & Monin, J.-L. 2003, *A&A*, 400, 185
- Madhusudhan, N., Amin, M. A., & Kennedy, G. M. 2014, *ApJL*, 794, L12
- Maldonado, J., Villaver, E., Eiroa, C., & Micela, G. 2019, *A&A*, 624, A94
- Mercer, A., Stamatellos, D., & Dunhill, A. 2018, *MNRAS*, 478, 3478
- Meru, F., & Bate, M. R. 2010, *MNRAS*, 409, 858
- Meru, F., & Bate, M. R. 2011a, *MNRAS*, 410, 559
- Meru, F., & Bate, M. R. 2011b, *MNRAS*, 411, L1
- Meru, F., Juhasz, A., Ilee, J. D., et al. 2017, *ApJL*, 839, L24
- Mizuno, H. 1980, *Prog. Theor. Phys.*, 64, 544
- Muller, S., Helled, R., & Mayer, L. 2018, *ApJ*, 854, 112
- Narang, M., Manoj, P., Furlan, E., et al. 2018, *AJ*, 156, 221
- Nayakshin, S. 2010, *MNRAS*, 408, L36
- Nelson, A. F. 2006, *MNRAS*, 373, 1039
- Nero, D., & Bjorkman, J. E. 2009, *ApJ*, 702, L163
- Nixon, C. J., King, A. R., & Pringle, J. E. 2018, *MNRAS*, 477, 3273

- Pollack, J. B., Hubickyj, O., Bodenheimer, P., et al. 1996, *Icarus*, 124, 62
- Rice, W. K. M., Armitage, P. J., Bate, M. R., & Bonnell, I. A. 2003, *MNRAS*, 339, 1025
- Rice, K., Lopez, E., Forgan, D., & Biller, B. 2015, *MNRAS*, 454, 1940
- Rogers, P. D., & Wadsley, J. 2012, *MNRAS*, 423, 1896
- Ruffert, M., & Arnett, D. 1994, *ApJ*, 427, 351
- Santos, N. C., Adibekyan, V., Figueira, P., et al. 2017, *A&A*, 603, A30
- Schlaufman, K. C. 2018, *ApJ*, 853, 37
- Stamatellos, D., & Whitworth, A. P. 2008, *A&A*, 480, 879
- Toomre, A. 1964, *ApJ*, 139, 1217
- Uyama, T., Hashimoto, J., Kuzuhara, M., et al. 2017, *AJ*, 153, 106
- Vorobyov, E. I. 2013, *A&A*, 552, A129
- Young, M. D., & Clarke, C. J. 2016, *MNRAS*, 455, 1438

Table 1. Initial conditions and results for the models, including the number of VPs lost to the inner and outer boundaries (δN_{VPi} and δN_{VPo} , respectively), and the total amount of disk mass lost to the central protostar or to VP formation and accretion (δM_d , in M_{Jup} units).

Model	β	final time (yrs)	final N_{VP}	maximum N_{VP}	δN_{VPi}	δN_{VPo}	δM_d
be1	1	288.	4	8	33	10	4.5
be2	3	407.	3	7	28	13	3.5
be3	10	391.	5	5	2	3	4.0
be4	20	447.	3	3	2	0	1.5
be5	30	422.	1	5	5	1	4.5
be6	40	462.	1	2	1	0	1.0
be7	50	450.	2	3	1	0	1.5
be8	100	417.	1	2	1	0	2.5

Table 2. Percentage of the total number of exoplanets in the present models (Figure 7) and from the Extrasolar Planets Encyclopedia observations (Figure 8) with masses above $0.1M_{Jup}$, sorted into separation bins of 2 au. The distributions are not inconsistent, considering the numerical bias for exoplanets near the finite radius outer edge of the numerical grid (20 au) and the observational bias against detections of long period orbits by transits or Doppler spectroscopy.

separation (au)	models (%)	observations (%)
4 - 6	28.	50.
6 - 8	31.	32.
8 - 10	19.	9.
10 - 12	7.	4.5
12 - 14	6.	0.
14 - 16	1.5	4.5
16 - 18	1.5	0.
18 - 20	6.	0.

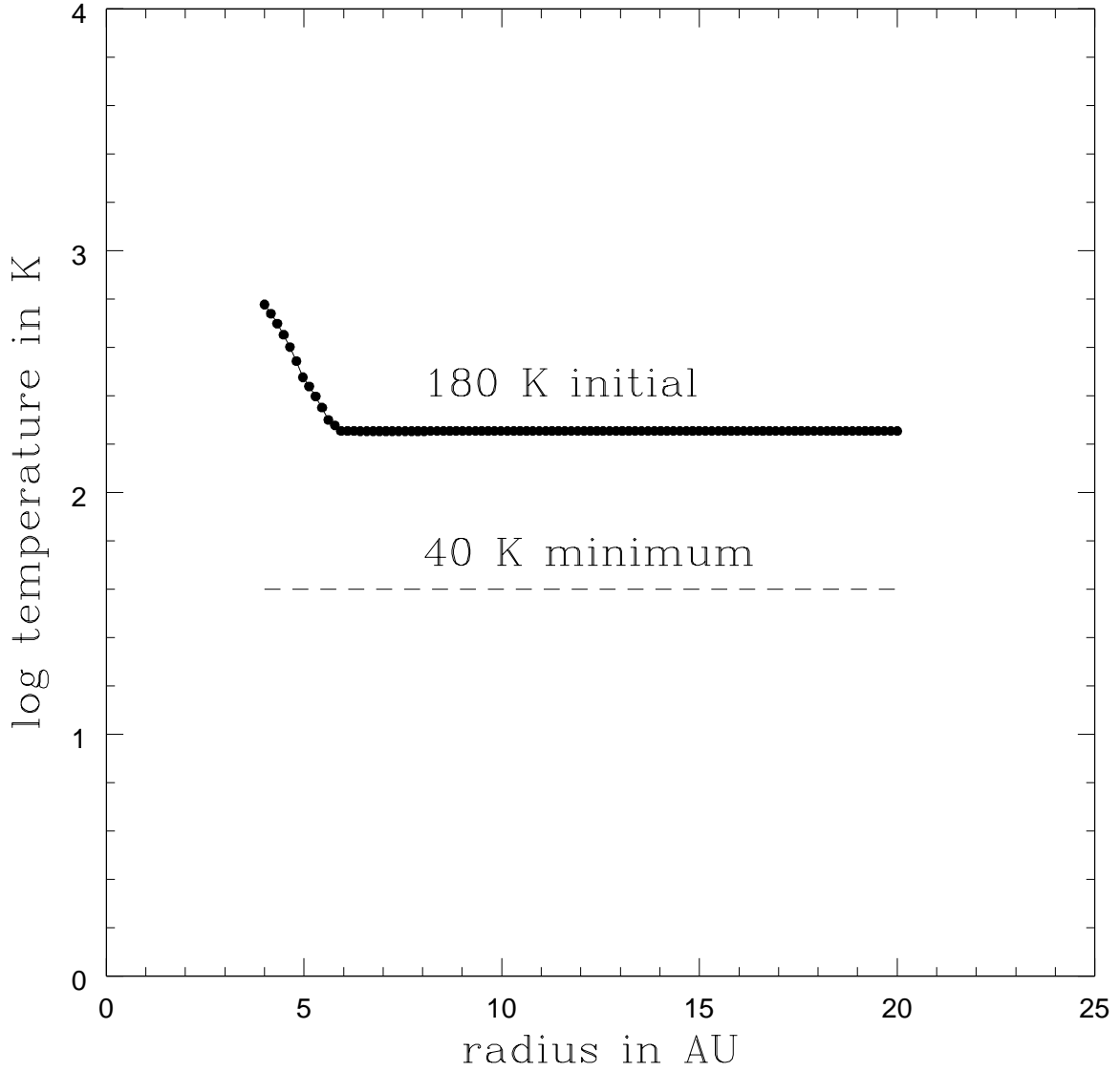


Fig. 1.— Initial midplane temperature profile for all the models, starting with an outer disk temperature of 180 K, leading to Toomre $Q = 2.7$ in the initially gravitational stable outer disk. The minimum outer disk temperature of 40 K, imposed during the evolutions, is also indicated.

See figure in pdf file below:

[https://aboss.dtm.carnegiescienc
e.edu/ftp-files
file name -- beta-evolve.pdf](https://aboss.dtm.carnegiescienc
e.edu/ftp-files
file name -- beta-evolve.pdf)

Fig. 2.— Equatorial (midplane) density contours for model be5 after (a) 38.5 yr, (b) 162 yr, (c) 318 yr, and (d) 422 yr. The disk has an inner radius of 4 au and an outer radius of 20 au. Contours are labelled in log cgs units. Maximum midplane gas densities at each time are: (a) 1.2×10^{-10} g cm $^{-3}$; (b) 2.6×10^{-9} g cm $^{-3}$; (c) 1.3×10^{-9} g cm $^{-3}$; and (d) 5.4×10^{-10} g cm $^{-3}$. The initial maximum midplane density is 1.0×10^{-10} g cm $^{-3}$.

See figure in pdf file below:

[https://aboss.dtm.carnegiescienc
e.edu/ftp-files
file name -- beta-evolve.pdf](https://aboss.dtm.carnegiescienc
e.edu/ftp-files
file name -- beta-evolve.pdf)

Fig. 3.— Equatorial (midplane) temperature contours for model be5 after (a) 38.5 yr, (b) 162 yr, (c) 318 yr, and (d) 422 yr, plotted as in Figure 2. Contours are labelled in log K units. The model starts with an initial minimum temperatures of 180 K (light orange color) and can cool down to a minimum temperature of 40 K (light green color).

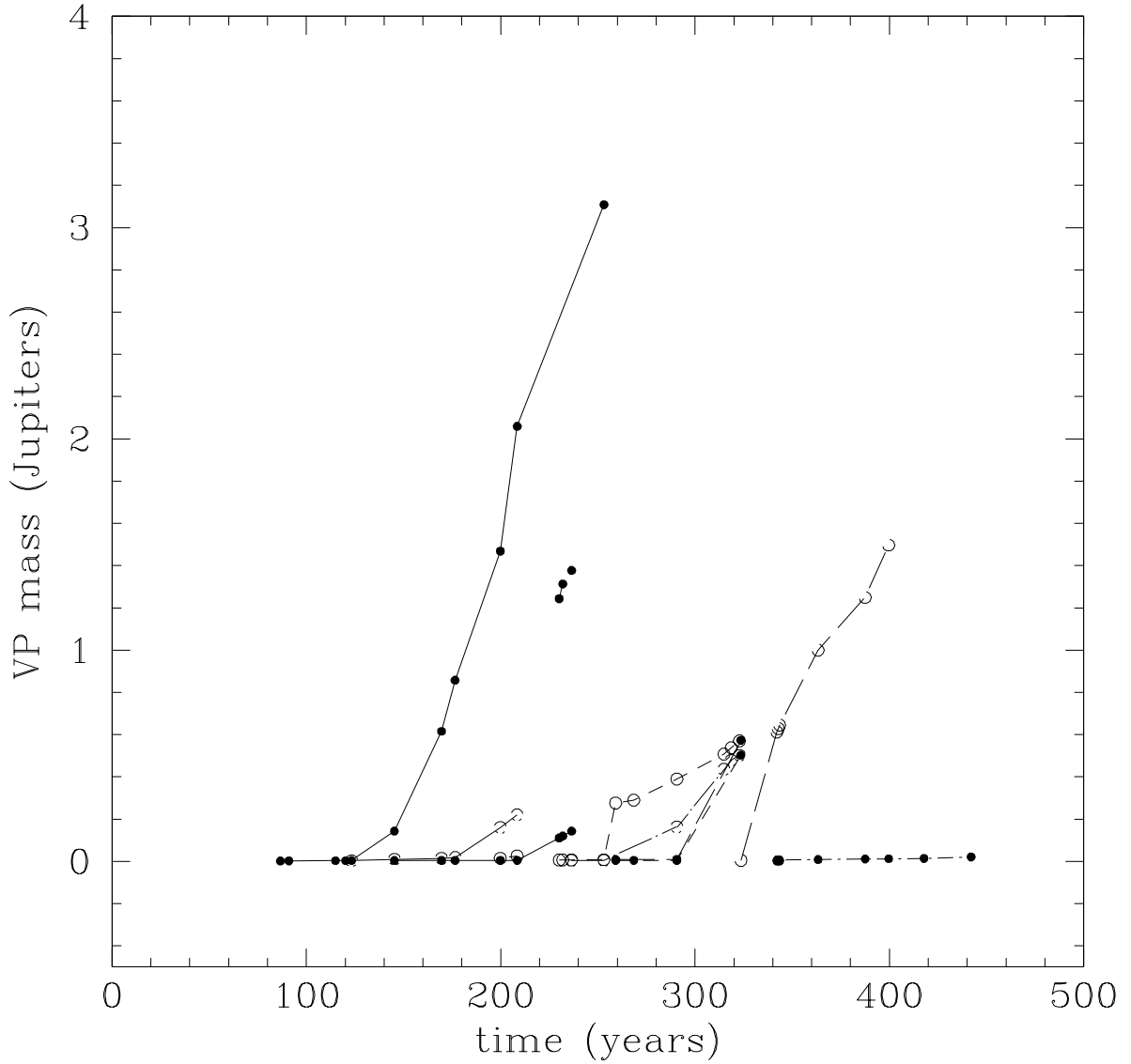


Fig. 4.— VP mass as a function of time for all of the VPs formed by model be5, with $\beta = 30$, sampled every 40,000 time steps throughout their evolutions. The VP masses increase by BHL accretion from the disk gas, while VPs that hit the inner (4 au) or outer (20 au) boundaries are removed from the evolutions. Differing symbols and lines are used to help delineate different VPs.

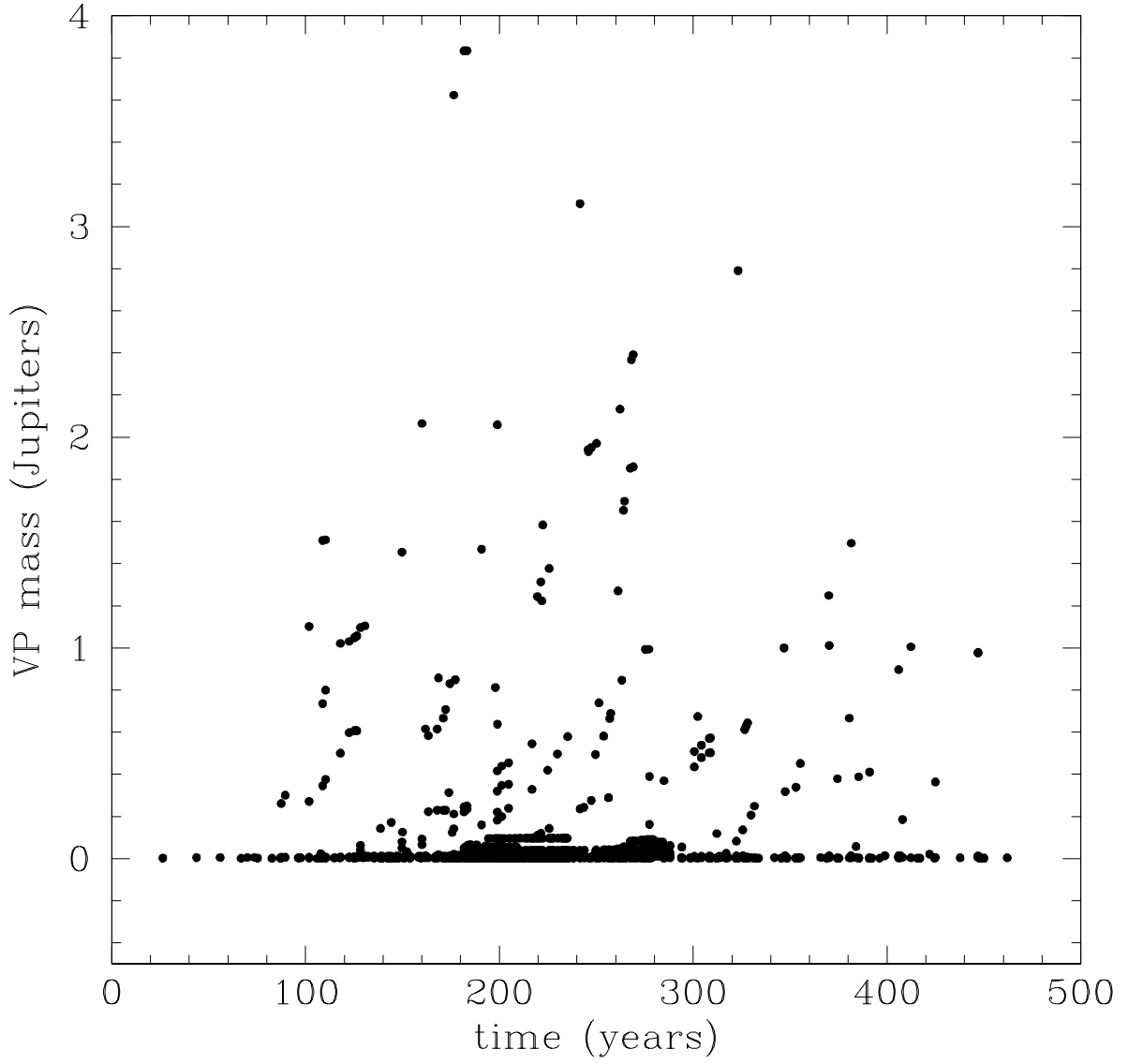


Fig. 5.— VP mass as a function of time for all of the VPs formed by all eight models in Table 1, plotted as in Figure 4.

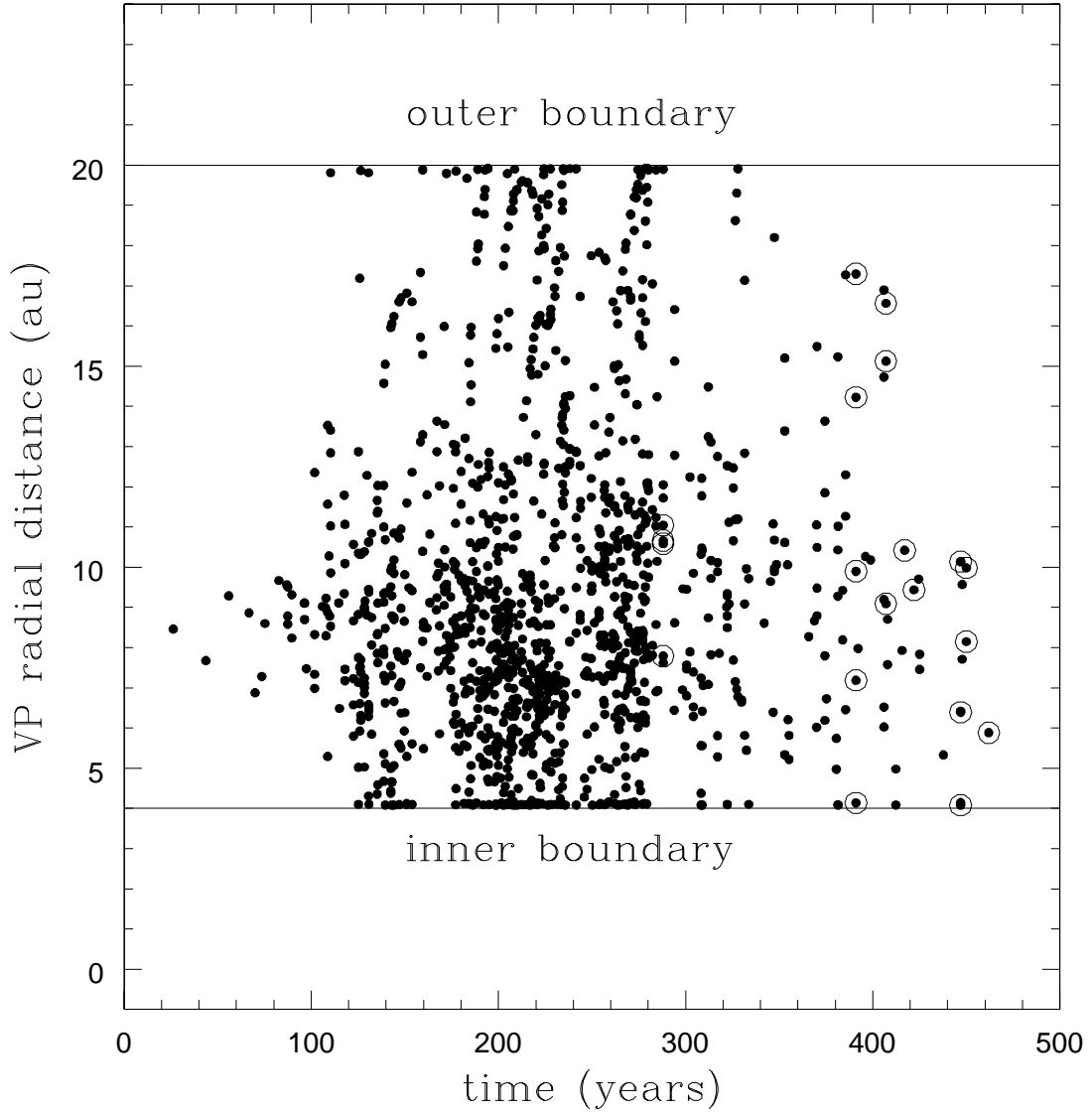


Fig. 6.— VP orbital radii as a function of time for all of the VPs formed by the eight models in Table 1, plotted as in Figure 4. The orbital radii both increase and decrease by disk migration and close encounters after forming in the ~ 6 au to 10 au region. VPs that hit the inner or outer boundaries are removed. Circled points designate the VP locations at culmination of each evolution.

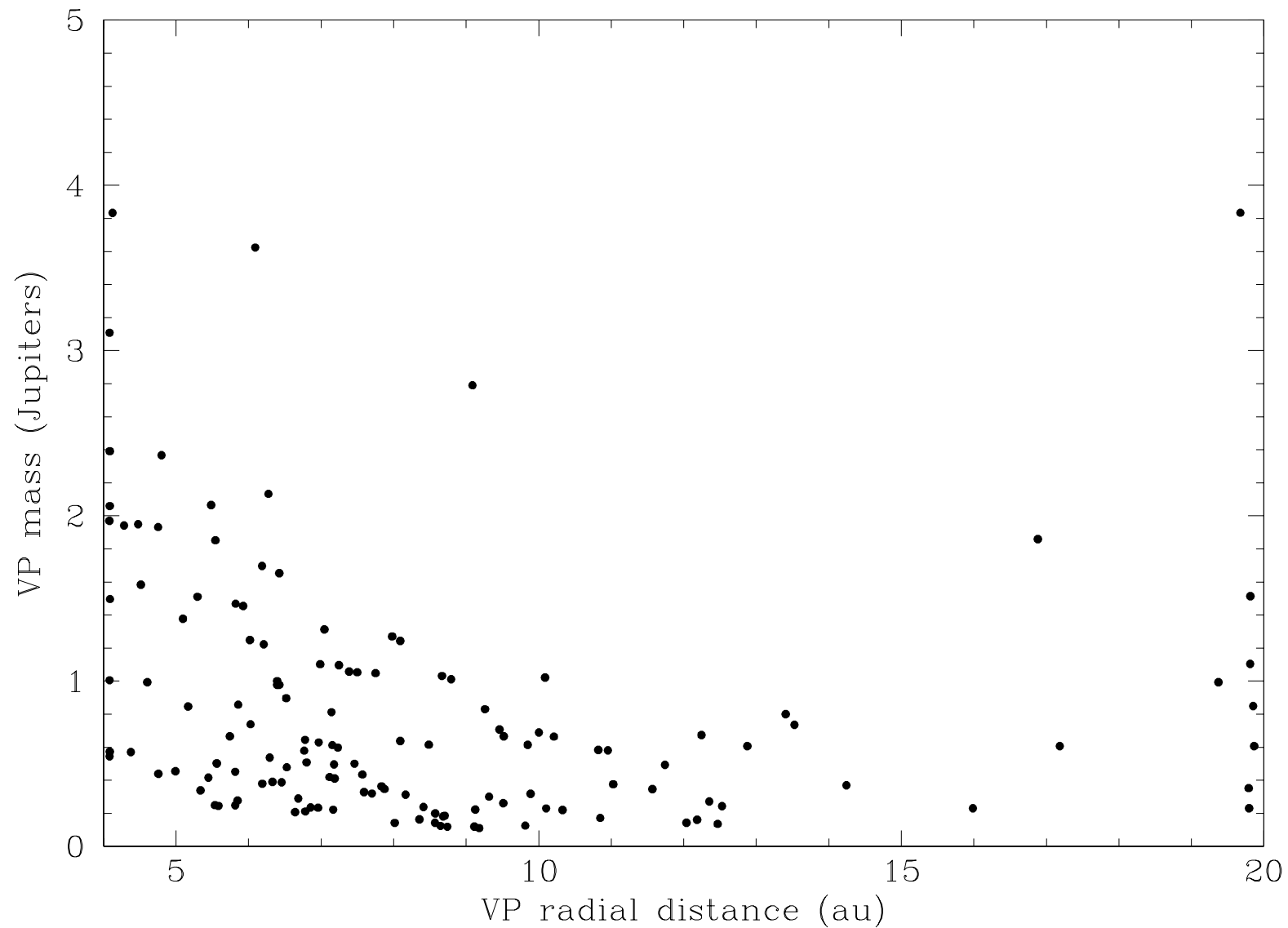


Fig. 7.— Masses and orbital radii of all of the VPs formed by the eight models in Table 1, sampled about 40 times throughout their evolutions, as in Boss (2017, Figure 9). The region plotted extends from 4 au to 20 au with masses between 0.1 and 5 M_{Jup} , for comparison (Table 2) with the observed exoplanets in Figure 8.

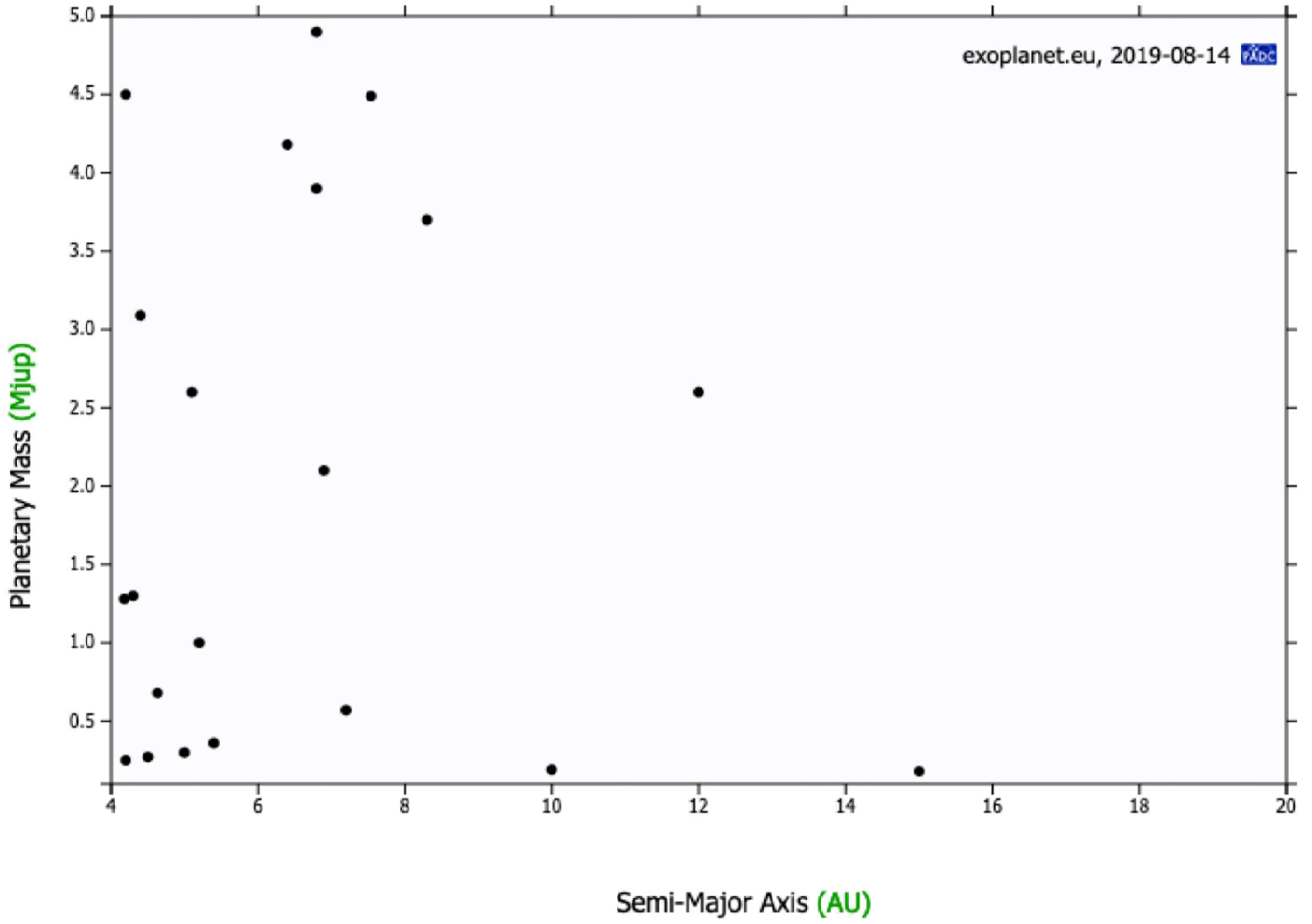


Fig. 8.— All exoplanets in the Extrasolar Planets Encyclopedia (exoplanets.eu) as of August 14, 2019, for masses between 0.1 and $5 M_{Jup}$ and semi-major axes between 4 au and 20 au, for comparison (Table 2) with the model results in Figure 7.